

ISAR Imaging Based on L1 L0 Norms Homotopy 2D Block Sparse Signal Recovery Algorithm

Changzheng Ma^{1, *}, Boon Poh Ng¹, and Jun Jie Feng²

Abstract—Many traditional sparse signal recovery based ISAR imaging methods did not utilize the block scatterers information of targets. Some block Bayesian learning based ISAR imaging algorithms are computational expensive. In this paper, a 2D block $\ell_1 \ell_0$ norms homotopy sparse signal recovery algorithm (the BL1L0 algorithm) is proposed and utilized to form the ISAR image. Compared with Bayesian-based algorithms, this algorithm can obtain ISAR images with similar image quality, but the computation speed is faster. Real data experiments verify the merits of our algorithm.

1. INTRODUCTION

Inverse synthetic aperture radar imaging has received much attention in the last three decades [1, 2]. Due to its “all day and all weather imaging” ability, ISAR imaging has been widely used in military and civilian fields. As ISAR transmitting wideband signals, scatterers on a target can be separated in the range direction via pulse compression technique. Due to the cross-range movement of the target relative to the radar, the scatterers on different cross-range positions have different relative Doppler frequencies. Using spectrum analysis, scatterers can then be separated in cross-range domain. The range and cross-range resolutions increase with the increase in bandwidth and Coherent Processing Interval (CPI) respectively. But the cross-range resolution can not be increased arbitrarily with the increase of CPI when Range-Doppler algorithm is used. One reason is that with the rotation of the target, scatterers will move through a range cell and coherent processing of the data is then not achievable by using the conventional Range-Doppler method. Another reason is that with the increase of the CPI, the rotation of the target may not be kept uniform, especially for maneuvering targets, conventional Fast Fourier Transform (FFT) based algorithm is not available. In order to improve the cross-range resolution in a short CPI, super-resolution method can be used.

By utilizing the sparse distribution of a signal, sparse signal recovery algorithm has the property of super-resolution and has been used in ISAR/SAR imaging [3–7]. In ISAR imaging, wide band signal processing can easily be implemented. After range compression and motion compensation (envelope alignment and phase compensation), the range profile signals can be expressed as $\mathbf{S} = \mathbf{A}\mathbf{E} + \mathcal{N}$, where \mathbf{S} , \mathbf{A} , \mathbf{E} and \mathcal{N} are the matrices corresponding to one dimensional range profiles, cross processing coefficients, scatterer amplitudes (ISAR image) and noise processes, respectively. The scatterers of man made targets are usually clusters or blocks. In order to use the block property of the scatterers, block sparse Bayesian learning based on Markov random fields and pattern-coupled sparse Bayesian learning (PC-SBL) algorithms are proposed [8–10]. However, these two methods are computational expensive, especially of [9], where forming a 128×64 ISAR image needs over one hour using a prevalent personal computer. $\ell_1 \ell_0$ norms homotopy based algorithm, by varying a parameter σ , builds a homotopy between ℓ_1 norm and ℓ_0 norm, and has superior performance [11, 12]. Another merit is that $\ell_1 \ell_0$ norms homotopy

Received 7 June 2016, Accepted 3 September 2016, Scheduled 19 September 2016

* Corresponding author: Changzheng Ma (eczma@gmail.com).

¹ School of Electrical and Electronic Engineering, Nanyang Technological University, Singapore. ² Nanjing University of Aeronautics and Astronautics, China.

algorithm is easily extended to 2D and block sparse signal recovery cases and the computation speed is fast. In this paper, ℓ_1 ℓ_0 norms homotopy algorithm is extended to the 2D signal model $\mathbf{S} = \mathbf{A}\mathbf{E} + \mathcal{N}$, where \mathbf{E} is assumed to be block sparse. Although the scatterers of the target are not regular block scatterers, in this paper, we assume that they can be approximated by small regular block scatterers. Real target imaging results show that this approximation is valid.

2. INVERSE SYNTHETIC APERTURE RADAR SIGNAL MODEL

Assume that the target is located in the far field and that the signal transmitted is a linear chirp signal:

$$s(t) = \mathbf{exp}\left(j2\pi\left(f_0t + \frac{1}{2}\mu_0t^2\right)\right), \quad t \in \left[-\frac{T}{2}, \frac{T}{2}\right], \quad (1)$$

where f_0 is the center frequency, μ_0 the chirp rate, and T the pulse duration. After mixing, the signal backscattered from a scatterer on the target can be expressed as $\alpha e^{-j2\pi f_0\tau(t) + j\pi\mu_0(t-\tau(t))^2}$, where $\tau(t)$ is the time delay, α is the signal amplitude. After range compression, the signal can be expressed as

$$s(t) = \alpha \mathbf{exp}(-j2\pi f_0\tau(t)) \mathbf{ sinc}(\mu_0 T(t - \tau(t))). \quad (2)$$

After envelope alignment and motion compensation, in a short CPI, the target can be regarded as rotating uniformly around an axis with rotation speed ω . Denote Y as the radar line of sight, Z the rotation axis of the target, (O, X, Y, Z) forms the right-hand coordinate system on the target, where O is the rotation origin. The initial position of a scatterer is (x_0, y_0, z_0) . Because the delay of a scatterer with a small z_0 has no relation with z_0 , we omit the z coordinate and assume that the scatterers are all located on the (X, Y) plane. The instantaneous position of the scatterer is $(x_0\mathbf{cos}(\omega t) - y_0\mathbf{sin}(\omega t), x_0\mathbf{sin}(\omega t) + y_0\mathbf{cos}(\omega t))$. The time delay is mainly determined by $x_0\mathbf{sin}(\omega t) + y_0\mathbf{cos}(\omega t)$. By Taylor expression and omitting the high order terms, $x_0\mathbf{sin}(\omega t) + y_0\mathbf{cos}(\omega t)$ can be expressed as

$$x_0\mathbf{sin}(\omega t) + y_0\mathbf{cos}(\omega t) \approx y_0 + x_0\omega t. \quad (3)$$

Then the time delay $\tau(t)$ can be expressed as $\tau(t) \approx \tau_0 + \frac{2(y_0 + x_0\omega t)}{c}$, where τ_0 is the delay of the origin and c the speed of light. The signal at range unit $\tau_0 + \frac{2y_0}{c}$ can be expressed as

$$s(t) = \alpha e^{-\frac{j4\pi x_0\omega t}{\lambda}}, \quad (4)$$

where $\lambda = \frac{c}{f_0}$ is the wavelength, and α includes the initial phase term and the reflection coefficient. After discretization, the signal can be expressed as $s(n) = \alpha a(n)$, where $a(n) = e^{j2\pi f_d n}$, $f_d = \frac{-2x_0\omega d_t}{\lambda}$, d_t is the sampling interval. When there are multiple scatterers, the total received signals from one range unit can be expressed as

$$\mathbf{s} = \mathbf{A}\mathbf{e} + \mathbf{n}, \quad (5)$$

where the columns of \mathbf{A} , which are the basis functions (vectors), are composed of the set of vectors \mathbf{a} 's with different f_d , \mathbf{e} is a column vector composed of the reflection coefficient α of different scatterers, \mathbf{n} is the noise term. Because different range profile signals share a common coefficient matrix \mathbf{A} , by combining the signals from different range units as a matrix \mathbf{S} , the total signals can be expressed as

$$\mathbf{S} = \mathbf{A}\mathbf{E} + \mathcal{N}, \quad (6)$$

where \mathbf{E} is the matrix formed by the reflection coefficients of the scatterers on the target, that is the ISAR image. From the point of sparse signal recovery algorithm, this signal model is similar to the multiple measurement vectors (MMV) model. In the MMV model, the non-zero signals in all columns of \mathbf{E} have the same supporting set. However, in (6), generally speaking, the non-zero signals of two columns of \mathbf{E} have different supporting set. The non-zero signals of \mathbf{E} are irregular block sparse. This can be shown in Fig. 3, the ISAR image of a real Yak-42 plane.

3. ℓ_1 ℓ_0 NORMS HOMOTOPY BLOCK SPARSE SIGNAL RECOVERY ALGORITHM

Because the ISAR image is block sparse, it can be obtained by solving the following optimization problem:

$$\min_{\mathbf{E}} \|\mathbf{E}\|_{bs} \quad s.t. \quad \|\mathbf{S}(:,n) - \mathbf{A}\mathbf{E}(:,n)\|_2 < \varepsilon, \quad n = 1, \dots, N \quad (7)$$

where $\|\cdot\|_{bs}$ expresses a block sparse norm of a matrix, and ε is the error bound due to noise and model error, N the number of columns of \mathbf{E} .

The scatterers of ISAR images are distributed as clusters, and the block character is not regular. Defining a block sparse norm of a non-regular block sparse signal is difficult, especially when the non-regular block character is unknown. In this paper, we combine the pixels as small regular blocks, then define a sparse norm for regular block sparse signals.

For a one dimensional sparse signal \mathbf{e} , define an exponential function $g_\sigma(e) = e^{-\frac{|e|}{\sigma}}$ and a sparse pseudo norm $G_\sigma(\mathbf{e}) = M - \sum_m g_\sigma(e(m))$ [12, 13], where M is the length of \mathbf{e} . It had been shown that when σ approaches $+\infty$, $G_\sigma(\mathbf{e})$ approaches ℓ_1 norm with a ratio difference; when σ approaches 0, $G_\sigma(\mathbf{e})$ approaches ℓ_0 norm. Hence, when σ moves from $+\infty$ to 0, $G_\sigma(\mathbf{e})$ moves smoothly from ℓ_1 norm to ℓ_0 norm.

For a one dimensional block sparse signal, assume that the signal vector \mathbf{e} can be expressed as $\mathbf{e} = [e_1, \dots, e_d, e_{d+1}, \dots, e_{2d}, \dots, e_{Pd}]$, where P is the number of blocks, every d elements are considered as a block, i.e., elements in a block have non-zero values (big values) or zero values (small values) at the same time. Block ℓ_1 norm and block ℓ_0 norm can be expressed as $\|\mathbf{e}\|_{b1} = \sum_{p=1}^P \sqrt{\sum_{i=1}^d |e((p-1)d+i)|^2}$ and $\|\mathbf{e}\|_{b0} = \sum_{p=1}^P I(\sum_{i=1}^d |e((p-1)d+i)|^2)$, where $I(e) = 1$ for $e \neq 0$ and $I(e) = 0$ for $e = 0$. Similarly, $G_\sigma(\mathbf{e})$ for block \mathbf{e} can be expressed as

$$G_\sigma(\mathbf{e}) = P - \sum_{p=1}^P g_\sigma \left(\sqrt{\sum_{i=1}^d |e((p-1)d+i)|^2} \right). \quad (8)$$

Steepest descent algorithm is usually used in finding the minimum point of a non-constraint optimization cost function. For linear constraint equations $\mathbf{s} = \mathbf{A}\mathbf{e}$, the feasible set is a linear subspace. Denote $\hat{\mathbf{e}}$ as an estimate of \mathbf{e} by using steepest descent algorithm. $\hat{\mathbf{e}}$ may do not belong to the feasible set. By letting $\tilde{\mathbf{e}} = \hat{\mathbf{e}} - \mathbf{A}^H(\mathbf{A}\mathbf{A}^H)^{-1}(\mathbf{A}\hat{\mathbf{e}} - \mathbf{s})$, then $\tilde{\mathbf{e}}$ satisfies $\mathbf{s} = \mathbf{A}\tilde{\mathbf{e}}$, i.e., $\tilde{\mathbf{e}}$ belongs to the feasible set. For the inequality constraint $\|\mathbf{s} - \mathbf{A}\mathbf{e}\|_2 < \varepsilon$, projection on the boundary of the feasible set is difficult, but because the feasible set of $\mathbf{s} = \mathbf{A}\mathbf{e}$ belongs to the feasible set of $\|\mathbf{s} - \mathbf{A}\mathbf{e}\|_2 < \varepsilon$, we can project $\hat{\mathbf{e}}$ on the feasible set of the equality constraint instead of the inequality constraint.

Similar to the smoothed ℓ_0 norm procedure for Single Measurement Vector (SMV) signal model, the ℓ_1 norm ℓ_0 norm homotopy sparse signal recovery algorithm for MMV signal model can be described as:

ℓ_1 norm ℓ_0 norm homotopy 2D block sparse signal recovery algorithm (BL1L0)

(i) Initialization:

- (a) Define constants L_0, L_1, J, ε , where L_0, L_1 determine the searching steps, J is the iteration numbers, choose a suitable decreasing sequence $[\sigma_1, \dots, \sigma_J]$, $\sigma_{i+1} = \rho\sigma_i$, $\rho < 1$.
- (b) Let $\hat{\mathbf{E}}_0$ be the minimum ℓ_2 norm solution of $\mathbf{S} = \mathbf{A}\mathbf{E}$, obtained by $\hat{\mathbf{E}}_0 = \mathbf{A}^\dagger \mathbf{S}$, where \dagger is the pseudo inverse.

(ii) for $j = 1, \dots, J$:

- (a) Let $\sigma = \sigma_j$, $\mathbf{E} = \hat{\mathbf{E}}_{j-1}$.
- (b) Let $\boldsymbol{\delta}$ be the gradient of $G_\sigma(\mathbf{E})$, $\mu = \min(E_{\max}/L_0, \sigma_j/L_1)$, where E_{\max} is the maximum value of $|\mathbf{E}|$.
- (c) For every element of \mathbf{E} , let $\mathbf{E}(m, n) \leftarrow \mathbf{E}(m, n) - \frac{\boldsymbol{\delta}(m, n)}{|\boldsymbol{\delta}(m, n)|} \times \min(|\mathbf{E}(m, n)|, |\mu\sigma_j\boldsymbol{\delta}(m, n)|)$.

- (d) If $\|\mathbf{A}\mathbf{E}(:,n) - \mathbf{S}(:,n)\|_2 > \varepsilon$, project $\mathbf{E}(:,n)$ back into the feasible set: $\mathbf{E}(:,n) \leftarrow \mathbf{E}(:,n) + \mathbf{A}^H(\mathbf{A}\mathbf{A}^H)^{-1}(\mathbf{S}(:,n) - \mathbf{A}\mathbf{E}(:,n))$.
- (e) Set $\hat{\mathbf{E}}_j = \mathbf{E}$.
- (iii) Final answer is $\hat{\mathbf{E}} = \hat{\mathbf{E}}_J$

The descent searching in this program is different from the conventional steepest descent algorithm. Fig. 1 shows a simple example in two-dimensional case. Denote point Q the sparsest solution. P_1 is a start searching point in the feasible set. P_2 is the next searching point using steepest descent algorithm. However, because the x coordinate changes from a positive value to a negative value when moves from P_1 to P_2 , we force its x coordinate to be zero. This means that the next searching point is P_3 . Because P_3 does not belong to the feasible set, it should be projected to P_4 , which belongs to the feasible set.

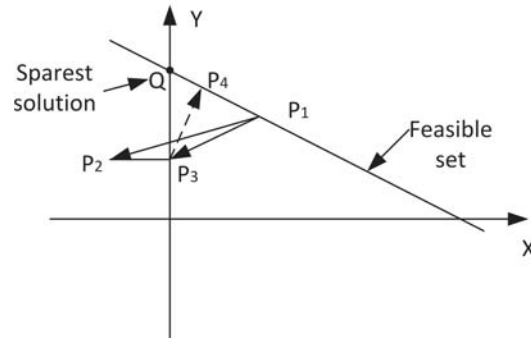


Figure 1. Descent search and projection on feasible set.

One important factor in steepest descent method is the design of step size. If the cost function is a smoothed convex function, by approximating the cost function with a quadratic function, an appropriate step size can be obtained by searching the minimum point of the quadratic function. But the cost function G_σ is not a convex function for a finite σ , there is no method to select an appropriate step size. For a large step size, it may not converge, but for a very small step size, the computation efficiency is low. Taking the minimum value, $\min(|\mathbf{E}(m,n)|, |\mu\sigma_j\boldsymbol{\delta}(m,n)|)$, ensures that the step size is not too big.

In the following, we discuss the selection criteria of the parameters $\sigma_1, \sigma_j, L_0, L_1$ and ε . Denote the dimension of matrix \mathbf{A} as $M \times N$. If there is only one isolated scatterer in one range unit with amplitude α , the maximum value of the initial estimate $\hat{\mathbf{E}}_0 = \mathbf{A}^\dagger \mathbf{S}$ will be approximately $\alpha M/N$. For the definition of the block cost function, $G_\sigma(\mathbf{e}) = P - \sum_p g_\sigma(\sqrt{\sum_{i=1}^d |e((p-1)d+i)|^2})$, $\sqrt{\sum_{i=1}^d |e((p-1)d+i)|^2}$ is the ℓ_2 norm of one block. Denote \hat{e}_{dmax} the maximum value of the ℓ_2 norm of the blocks of $\hat{\mathbf{E}}$. Then σ_1 should be larger than $\hat{e}_{\text{dmax}}N/M$. σ_j can be chosen as σ_1/L , where L can be chosen as $50 \sim 100$, which is related with the expected dynamic range of the image.

For ISAR imaging, the noise variance $\hat{\varepsilon}$ can be estimated from the range profiles. Then ε can be chosen as $2M\hat{\varepsilon}$.

Generally speaking, the step size μ is only related with σ_j , such as letting $\mu = \sigma_j/L_1$. However, because σ_1 is larger than $\hat{e}_{\text{dmax}}N/M$ at the first few iterations, the descent movement step length $|\mu\sigma_j\boldsymbol{\delta}(m,n)|$ may be larger than the value of the signal $\mathbf{E}(m,n)$, then $\min(|\mathbf{E}(m,n)|, |\mu\sigma_j\boldsymbol{\delta}(m,n)|)$ may equal $|\mathbf{E}(m,n)|$. Then $\mathbf{E}(m,n) - \frac{\boldsymbol{\delta}(m,n)}{|\boldsymbol{\delta}(m,n)|} \times \min(|\mathbf{E}(m,n)|, |\mu\sigma_j\boldsymbol{\delta}(m,n)|)$ will be zero. After projection $\mathbf{E}(:,n) \leftarrow \mathbf{E}(:,n) + \mathbf{A}^H(\mathbf{A}\mathbf{A}^H)^{-1}(\mathbf{S}(:,n) - \mathbf{A}\mathbf{E}(:,n))$, $\mathbf{E}(:,n) = \mathbf{A}^H(\mathbf{A}\mathbf{A}^H)^{-1}\mathbf{S}(:,n)$, which is still the minimum ℓ_2 norm estimation. This means that after one iteration, the searching point returns to the starting point. By choosing L_0 to be a large value, such as 20, and letting $\mu = \min(E_{\text{max}}/L_0, \sigma_j/L_1)$, we can ensure that the next searching point does not equal to the last searching point at the first few searching steps.

In the following, we discuss the choice of L_1 . We explain it by no-block signal case. The gradient of $g_\sigma(e)$, denoted as δ , is $-e^{-\frac{|e|}{\sigma}} \frac{\text{sign}(e)}{\sigma}$. $\sigma\delta$ is $-e^{-\frac{|e|}{\sigma}} \text{sign}(e)$. When e is much smaller than σ , $\sigma\delta$ approximately equals ± 1 . Then the term $|\mu\sigma_j\delta|$ will be larger than $|e|$ and $e \leftarrow e - \frac{\delta}{|\delta|} \times \min(|e|, |\mu\sigma_j\delta|)$ will be zero. When e is much larger than σ , $e^{-\frac{|e|}{\sigma}}$ is a small value, in the descent movement step, it moves a very small step. So the most efficient time that e converges to the true value is when σ approximates e . Assume K iterations are needed for σ changes from σ_1 to $\sigma_1/2$, then $\sigma_1/2 = \sigma_1 \times \rho^K$, that is $K = \frac{-1}{\log_2(\rho)}$. Without considering projection, K descent movement steps move about $K(\frac{\sigma}{L_1}e^{-1})$. Let $K(\frac{\sigma}{L_1}e^{-1})$ equal σ , we have $L_1 = Ke^{-1}$. Sometimes, when the number of iterations is chosen as a small value, L_1 will be a small value. This will give rise to a big step size and affect the convergence. In real implementations, we can choose $L_1 = \max(25, Ke^{-1})$ to ensure that L_1 is not too small.

4. SIMULATION RESULTS

In this section, a set of real data of a Yak-42 aircraft is used to demonstrate the performance of the proposed sparse signal recovery algorithm. The Yak-42 aircraft, which is shown in Fig. 2, has an uptilted tail and its length/width/height are 36.38 m/34.2 m/9.83 m, respectively. The distance of the aircraft to the radar is about 33.5 km and the height is about 5 km. The carrier frequency is on the C band with signal bandwidth of 400 MHz, corresponding to a range resolution of 0.375 m. The pulse repetition frequency is 100 Hz. 256 pulses within dwell time $[-1.28, 1.28]$ s are used in conventional FFT method and the ISAR image is shown in Fig. 3.

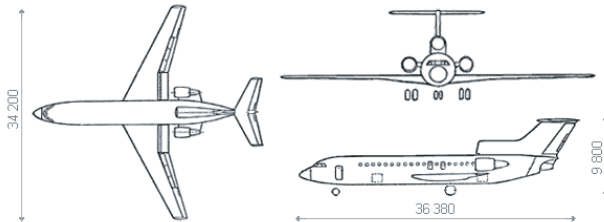


Figure 2. The shape of the Yak-42 plane.

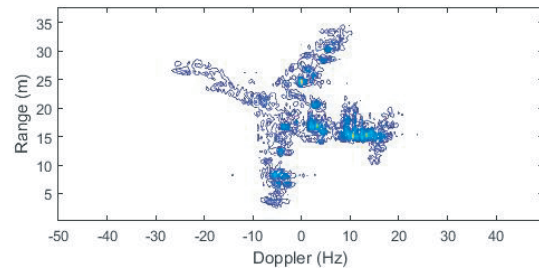


Figure 3. ISAR image using FFT method and 256 pulses.

Fig. 4 and Fig. 5 show the ISAR images using PC-SBL (the comparison between PC-SBL and other methods can be referred in [10]) and BL1L0 algorithm with pulses of 16 and 32. The Matlab program of PC-SBL is downloaded from <http://www.junfang-uestc.net/codes/ISAR.rar>. For the PC-SBL algorithm, the parameters used are the default parameters in the downloaded program, where $\beta = 1$, four contiguous range profiles are combined as the data of a MMV equation. Even though the original PC-SBL algorithm can process more contiguous range profiles at one time, due to the huge coefficient matrix formed, [10] used four contiguous range profiles to save memories and computations. For the BL1L0 algorithm, as in [3], the noise level is estimated from the range profiles, that is, using range cells from 1 to 25 to estimate the noise variance. L_0 is chosen as 20, $\sigma_1 = N/M\hat{e}_{dmax} \times 8$, $\sigma_J = \sigma_1/60$. For every implementation, 500 iterations are used to recover the image. The ISAR image is divided as 4×2 small blocks, where 4 expresses 4 cross-range units. It can be seen that the image qualities are similar for the two methods. For both cases, the ISAR images using the BL1L0 algorithm show more information about the neck of the target, and at the same time, it seems that the edges of the wing of the BL1L0 ISAR images are clearer. Because the PC-SBL method does not assume the shape of the block, it is more flexible. The computation time using the BL1L0 method for 16 and 32 pulses are all about 53s, but 135s and 77s respectively, for the PC-SBL method. It can be seen that the BL1L0 algorithm is computational economical.

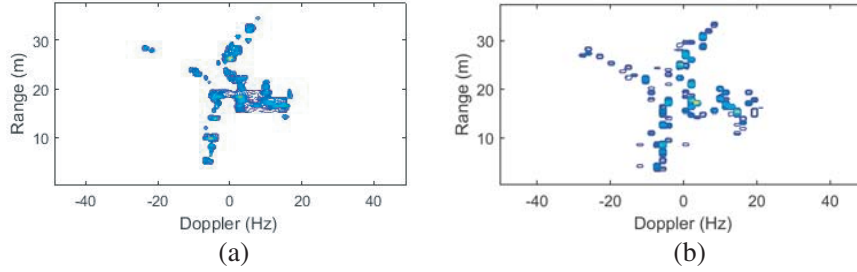


Figure 4. ISAR image using 16 pulses. (a) PC-SBL algorithm. (b) BL1L0 algorithm, the block size is 4×2 , where 4 expresses 4 cross-range units.

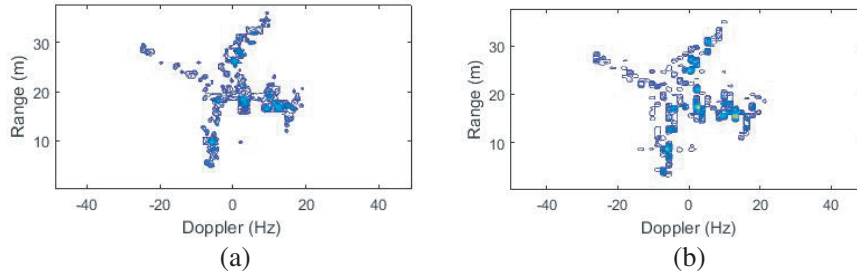


Figure 5. ISAR image using 32 pulses. (a) PC-SBL algorithm. (b) BL1L0 algorithm, the block size is 4×2 , where 4 expresses 4 cross-range units.

5. CONCLUSION

For ISAR imaging, range profiles are formed at first, then after envelope alignment and motion compensation, the range profiles form a two-dimensional matrix. In this paper, a two-dimensional block sparse signal recovery algorithm based on MMV signal model is used to form the ISAR image. Although the block is not regular, using a small regular block signal model can improve the image quality.

REFERENCES

1. Mensa, D. L., *High Resolution Radar Cross-Section Imaging*, Artech House, 1991.
2. Wehner, D. R., *High Resolution Radar*, Artech House, 1994.
3. Zhang, L., M. Xing, C. W. Qiu, J. Li, and Z. Bao, "Achieving higher resolution ISAR imaging with limited pulses via compressed sampling," *IEEE Geosci. Remote Sens. Lett.*, Vol. 6, No. 3, 567–571, 2009.
4. Jiang, C., B. Zhang, J. Fang, Z. Zhe, W. Hong, Y. Wu, and Z. Xu, "Efficient l_q regularisation algorithm with range-azimuth decoupled for SAR imaging," *Electronics Letters*, Vol. 50, No. 3, 204–205, 2014.
5. Cetin, M., I. Stojanovic, N. Onhon, K. R. Varshney, S. Samadi, W. C. Karl, and A. S. Willsky, "Sparsity-driven synthetic aperture radar imaging," *IEEE Signal Processing Magazine*, Vol. 31, No. 4, 27–40, 2014.
6. Zhang, X., T. Bai, H. Meng, and J. Chen, "Compressive sensing-based ISAR imaging via the combination of the sparsity and nonlocal total variation," *IEEE Geoscience and Remote Sensing Letters*, Vol. 11, No. 5, 990–994, 2014.
7. Lv, J., L. Huang, Y. Shi, and X. Fu, "Inverse synthetic aperture radar imaging via modified smoothed l_0 norm," *IEEE Antennas and Wireless Propagation Letters*, Vol. 13, 1235–1238, 2014.

8. Wang, L., L. Zhao, G. Bi, C. Wan, and L. Yang, "Enhanced ISAR imaging by exploiting the continuity of the target scene," *IEEE Transactions on Geoscience and Remote Sensing*, Vol. 52, No. 9, 5736–5750, 2014.
9. Wang, L., L. Zhao, G. Bi, and C. Wan, "Sparse representation-based ISAR imaging using Markov random fields," *IEEE Journal of Selected Topics in Applied Earth Observations and Remote Sensing*, Vol. 8, No. 8, 3941–3953, 2015.
10. Duan, H., L. Zhang, J. Fang, L. Huang, and H. Li, "Pattern-coupled sparse Bayesian learning for inverse synthetic aperture radar imaging," *IEEE Signal Processing Letters*, Vol. 22, No. 11, 1995–1999, 2015.
11. Mohimani, H., M. Babaie-Zadeh, and C. Jutten, "A fast approach for overcomplete sparse decomposition based on smoothed ℓ_0 norm," *IEEE Trans. Signal Process.*, Vol. 57, No. 1, 289–301, 2009.
12. Ma, C., T. Yeo, Y. Zhao, and J. Feng, "MIMO radar 3D imaging based on combined amplitude and total variation cost function with sequential order one negative exponential form," *IEEE Trans. Image Process.*, Vol. 23, No. 5, 2168–2183, 2014.
13. Ma, C., T. S. Yeo, Z. Liu, Q. Zhang, and Q. Guo, "Target imaging based on $\ell_1 \ell_0$ norms homotopy sparse signal recovery and distributed MIMO antennas," *IEEE Transactions on Aerospace and Electronic Systems*, Vol. 51, No. 4, 3399–3414, 2015.